

Article

# Exploring the Potential of WorldView-2 Red-Edge Band-Based Vegetation Indices for Estimation of Mangrove Leaf Area Index with Machine Learning Algorithms

Yuanhui Zhu <sup>1</sup>, Kai Liu <sup>1,\*</sup> , Lin Liu <sup>2,3,\*</sup>, Soe W. Myint <sup>4</sup>, Shugong Wang <sup>5</sup>, Hongxing Liu <sup>3</sup> and Zhi He <sup>1</sup>

<sup>1</sup> Center of Integrated Geographic Information Analysis, Guangdong Key Laboratory for Urbanization and Geo-Simulation, School of Geography and Planning, Sun Yat-sen University, Guangzhou 510275, China; zhuyuhui2@mail3.sysu.edu.cn (Y.Z.); hzhdhz@126.com (Z.H.)

<sup>2</sup> Center of Geographic Information Analysis for Public Security, School of Geographic Sciences, Guangzhou University, Guangzhou 510006, China

<sup>3</sup> Department of Geography, University of Cincinnati, Cincinnati, OH 45221-0131, USA; Hongxing.Liu@uc.edu

<sup>4</sup> School of Geographical Sciences and Urban Planning, Arizona State University, Tempe, AZ 85287-5302, USA; Soe.Myint@asu.edu

<sup>5</sup> Guangdong Key Laboratory of Geological Processes and Mineral Resources Survey, School of Earth Science and Geological Engineering, Sun Yat-sen University, Guangzhou 510275, China; esswsg@mail.sysu.edu.cn

\* Correspondence: liuk6@mail.sysu.edu.cn (K.L.); Lin.Liu@uc.edu (L.L.); Tel.: +86-020-8411-3044 (K.L.); +1-513-556-3429 (L.L.); Fax: +86-020-8411-3057 (K.L. & L.L.)

Received: 15 August 2017; Accepted: 15 October 2017; Published: 18 October 2017

**Abstract:** To accurately estimate leaf area index (LAI) in mangrove areas, the selection of appropriate models and predictor variables is critical. However, there is a major challenge in quantifying and mapping LAI using multi-spectral sensors due to the saturation effects of traditional vegetation indices (VIs) for mangrove forests. WorldView-2 (WV2) imagery has proven to be effective to estimate LAI of grasslands and forests, but the sensitivity of its vegetation indices (VIs) has been uncertain for mangrove forests. Furthermore, the single model may exhibit certain randomness and instability in model calibration and estimation accuracy. Therefore, this study aims to explore the sensitivity of WV2 VIs for estimating mangrove LAI by comparing artificial neural network regression (ANNR), support vector regression (SVR) and random forest regression (RFR). The results suggest that the RFR algorithm yields the best results ( $RMSE = 0.45$ , 14.55% of the average LAI), followed by ANNR ( $RMSE = 0.49$ , 16.04% of the average LAI), and then SVR ( $RMSE = 0.51$ , 16.56% of the average LAI) algorithms using 5-fold cross validation (CV) using all VIs. Quantification of the variable importance shows that the VIs derived from the red-edge band consistently remain the most important contributor to LAI estimation. When the red-edge band-derived VIs are removed from the models, estimation accuracies measured in relative RMSE (RMSE<sub>r</sub>) decrease by 3.79%, 2.70% and 4.47% for ANNR, SVR and RFR models respectively. VIs derived from red-edge band also yield better accuracy compared with other traditional bands of WV2, such as near-infrared-1 and near-infrared-2 band. Furthermore, the estimated LAI values vary significantly across different mangrove species. The study demonstrates the utility of VIs of WV2 imagery and the selected machine-learning algorithms in developing LAI models in mangrove forests. The results indicate that the red-edge band of WV2 imagery can help alleviate the saturation problem and improve the accuracy of LAI estimation in a mangrove area.

**Keywords:** WorldView-2 imagery; vegetation index; leaf area index; red-edge band; variable importance; mangrove forests; machine learning

## 1. Introduction

Mangrove ecosystems are regarded as one of the most productive ecosystems on earth with long-term storage of abundant biomass and organic carbon [1]. Mangrove forests provide a number of ecosystem services [2], such as protection of the coastline from storm surges and tsunamis, reduction of coastal erosion, decreased coastal pollution, and formation of nursery areas for a variety of terrestrial and aquatic fauna [3–5]. Globally, coastal areas are commonly associated with high-density population pressure and urban growth [6], and this has resulted in the conversion of mangrove ecosystems into areas for aquaculture, salt production, and rice cultivation over the past few decades [7–9]. The consequence has been widespread deforestation of mangroves.

Artificial planting of mangrove forests has been used to restore and rehabilitate mangrove forests in China since the 1990s [10]. Comprehensive monitoring of the recovery process and its effects on mangrove ecosystems can increase understanding of mangrove net primary production, photosynthesis, and plant health [11,12]. As a key biophysical parameter, the leaf area index (LAI) is an important input parameter in dynamic global vegetation models [13–16], and studies of vegetation LAI can contribute to the understanding of vegetation conditions and ecological processes in general [17].

Compared to QuickBird and IKONOS images, WorldView-2 (WV2) imagery, with higher spatial and spectral resolution, provides great potential for estimating and mapping forest biophysical parameters [18–20]. Although previous studies have demonstrated that the WV2 imagery can be successfully utilized for estimating and mapping forest structure parameters with a reasonable accuracy including canopy nitrogen concentration [21], biomass [22], tree crown [23], etc., few studies focused on prediction and mapping of forest LAI using WV2 imagery [24–27], especially for mangrove forests. Kamal et al. assessed multi-resolution images for mangrove LAI mapping and focused on exploring the relationship between image spatial resolution, sampling sizes and spatial variation for estimating LAI [25]. Therefore, more studies are needed to further investigate the application of WV2 imagery for LAI estimation.

Mangrove forests often have a great spatial variation in LAI values due to the impact of species types, stand density, and their growing environment [28]. They show distinctive spectral reflectance and absorption features affected by the soil and water surrounding compared to other forests [29]. However, understanding of mangrove LAI variations is relatively limited. Scholars have attempted to measure the LAI of mangrove forests using various types of sensors and models. For example, Kovacs et al. [16,30–33] successfully built the linear relationship between LAI values and parameters derived from different remote-sensing images (e.g., the bands or their spectral transformations, texture information, and backscattering coefficients) utilizing field survey data. They also assessed the health status of mangrove forests based on LAI variations of different species types. Wong et al. developed a stepwise regression model between measured LAI values of mangrove forests and vegetation indices (VIs), texture information, and backscattering coefficients combined with hyperspectral and radar images [34]. However, most studies have primarily focused on the linear relationship between LAI and remote sensing-derived parameters.

There exists no publication on the sensitivity of bands or spectral transformations for LAI estimation for mangrove forests using WV2 imagery. Previous studies have demonstrated that traditional bands and their spectral transformations from multi-spectral images are not sensitive to LAI variations [35,36]. The application of the above parameters may suffer from saturation effects for mangrove forests. Therefore, detailed and accurate estimation of mangrove LAI is still a challenge using multi-spectral sensors. Adjourlolo, Mutanga and Cho [21], Van Deventer et al. [37], Cho et al. [38], Mutanga et al. [39] found that the red-edge band from hyperspectral data, RapidEye or WV2 imagery can contribute to improving accuracies of estimation due to higher sensitivity to biochemical and biophysical parameters such as biomass, canopy nitrogen, and foliar N and P. The red-edge band was used to develop their optimal combination of attributes. However, Pu and Cheng [26] found that the red-edge band from WV2 imagery was considered the worst input variable in estimating LAI of mixed natural forests than other WV2 bands. There is no generally agreed conclusion on the effectiveness of

the red-edge band. Therefore, the sensitivity of the red-edge band in estimating LAI should be further explored using WV2 imagery in mangrove forests.

A number of scholars have explored different methods in estimating LAIs. LAI values are estimated primarily using two complementary groups of approaches (radiative transfer models and statistical models) from remotely sensed data [40]. Physically based radiative transfer models are used to inverse the LAI and other biophysical parameters [41–43]. Statistical models and machine-learning algorithms are commonly used to retrieve LAI values. However, statistical models, such as linear regression and logistic regression, require variables to follow certain statistical distributions (e.g., the normal distribution), which are often an over-simplification [44]. Machine-learning algorithms, including classification and regression trees (CART), artificial neural networks (ANN), support vector machines (SVM) and random forests (RF), can often reach a superior prediction accuracy due to fewer assumptions about the data and processes. Several studies have demonstrated that machine-learning algorithms are effective for modeling vegetation LAI using remotely sensed data and field measurements [45,46]. However, a single model has a certain randomness and instability partially due to the possible change in input variables performance during the calibration process [47].

The overall goal of the study is to evaluate the sensitivity of the red-edge band of WV2 imagery for mangrove forests with distinctive spectral reflectance features using different models. Comparisons of multiple models can help discern the pros and cons of each, eventually point to the direction of the best performing model [48]. Two questions are addressed in this study: (1) Are WV2 imagery and the selected machine-learning algorithms suitable for developing LAI estimation models in mangrove forests with high spatial heterogeneity? (2) What is the relative importance of the VIs in estimating mangrove LAI?

## 2. Materials and Methods

### 2.1. Study Area

Mangrove forests in Dawei Bay, with an area of about 700 ha, are located on northwest Qi’ao Island, near the City of Zhuhai in Guangdong Province [49] (Figure 1). The coastal region has an ideal setting for the growth of mangrove forests. The bay is located between latitude 22°23'N–22°27'N and longitude 113°36'E–113°39'E and has a subtropical monsoon climate with prevailing southeast winds in summer and northeast winds in winter. The average annual temperature is 22.4 °C, the annual average sunshine hours is 1907.4 h, and the average annual precipitation is between 1700 mm and 2200 mm [11,50]. The salinity of surface seawater ranges from 0.22‰ to 32.32‰ with an annual average of 18.22‰ [11,51]. The tidal pattern is an irregular semidiurnal tide. As a typical wetland ecosystem, mangrove forests in Dawei Bay have been designated a provincial-level nature reserve—the largest area of artificially planted mangrove forests in China.

Mangrove forests of Dawei Bay with high spatial heterogeneity grades, ranging from prevalent mature forest, to smaller trees and shrubs, and to herbaceous vegetation [50]. Dominant species include *Kandelia candel* (*K. candel*), *Aegiceras corniculatum* (*A. corniculatum*), *Acanthus ilicifolius* (*A. ilicifolius*), *Sonneratia apetala* (*S. apetala*), and *Acrostichum aureum* (*A. aureum*) [52]. The mature native *K. candel* and *A. corniculatum* are mostly located in the high tidal zones outside the enclosing levee. The other three mangrove species are distributed in the middle and low tidal zones. *S. apetala*, a fast-growing tree, has been artificially planted on the island since 1999 [50]. A large area dominated by the invasive species, *Spartina alterniflora* (*S. alterniflora*), is mainly distributed outside the intertidal flat and is designated as a reconstructed demonstration area. There are other species distributed in the region as well, including *Phragmites australis* (*P. australis*) as well as mangrove nurseries.

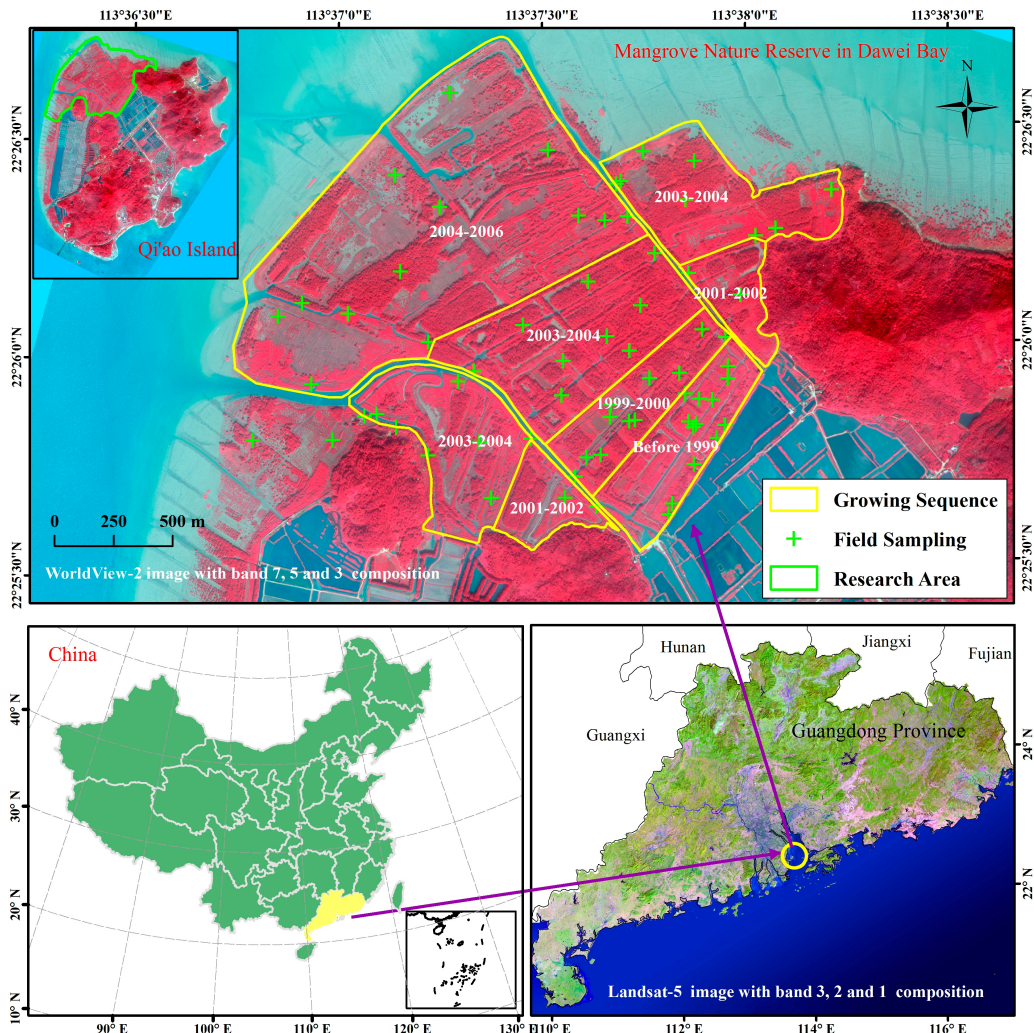


**Figure 1.** The study area and field sampling sites on Qi'ao Island overlaid on WV2 imagery.

## 2.2. Measurement of LAI

We obtained LAI values and mangrove species in the field survey. The LAI of mangrove forests was obtained by measuring the gap fraction in five zenith angles and Miller's theorem using the Plant Canopy Analyzer LAI-2000 (LI-COR Biosciences, Inc., Lincoln, NE, USA, 2010). The gap fraction is calculated from the ratio of above-canopy light intensity (A) and below-canopy light intensity (B) [53]. It has been demonstrated to be a practical method for obtaining LAI values [54,55]. Actually, the LAI obtained from LAI-2000 is an effective LAI and has been shortened to LAI henceforward.

There were a total of 68 rectangular plots located along tidal creeks, including 9, 6, 6, 14, 7, 6, 20 samples of *S. alterniflora*, *P. australis*, *A. aureum*, *A. ilicifolius*, *A. corniculatum*, *K. candel* and *S. apetala*, respectively. Mangrove forests within this dynamic landscape are characterized by uneven-aged trees and high spatial variability. The data of tree age was obtained by the conservation authority of mangrove nature preservation and mangrove growers. LAI variation was investigated based on different species types and age (growth stages) (Figure 1). The distribution of samples was selected to include all species in different growth stages in the study area to ensure that all LAI variations were represented in the samples. Two field surveys were conducted on the 23 and 27 of December 2010 and the 10 and 15 of January 2011. Each sample plot with a 10 m × 10 m quadrant was selected in a homogeneously covered species. Two line transects were made along the two diagonal lines of each sample plot using a cloth tape measure. For each diagonal line, five below-canopy readings and one

above-canopy reading were taken at regular intervals using a  $180^{\circ}$  view angle cap with a sensor to mask out the operator. Therefore, the LAI value in each sampling point was measured twice along with two diagonal lines. Finally, the mean LAI value was calculated from the two measurements.

The four vertex coordinates of each sampling point were recorded by a sub-meter accurate GPS. Further, auxiliary details such as distances to shore and other features that can easily be identified in the WV2 imagery were collected to mark in locating sites on the images.

The LAI values obtained from field study ( $n = 68$ ) varied from 1.77 to 6.01. The mean LAI value was 3.08, and the coefficient of variation was 0.45. The measured LAI values suggested mangrove forests exists the high degree of spatial variability.

### 2.3. Workflow for the Analyses

Three different regression models, including Artificial Neural Network regression (ANNR) [56], Support Vector Machine regression (SVMR) [57], and Random Forest regression (RFR) [44], were used to explore different models' performance and the sensitivity of VIs related to mangrove LAI. These methods have been successfully used in classification and retrieval of remotely sensed data and are capable of quantifying a variable's importance. Figure 2 provides the workflow for mapping LAI from WV2 imagery. The VIs, as predictor variables, were calculated after image processing. The LAI values and mangrove species were obtained from field investigations. The mangrove species map was obtained by using object-oriented classification and SVM algorithm. Then, the regression models (ANNR, SVR, and RFR algorithms) were selected to establish non-linear relationships between the LAI and the predictor variables. The constructed models were applied to the WV imagery to map the spatial distribution of LAI. The statistical analysis for predicted LAI map of each species were calculated based on mangrove species map. Variables' importance was determined to analyze the sensitivity of predictor variables. To quantify the contribution of red-edge band, we built different LAI estimating models with and without VIs derived from red-edge bands based on ANNR, SVR and RFR models, respectively.

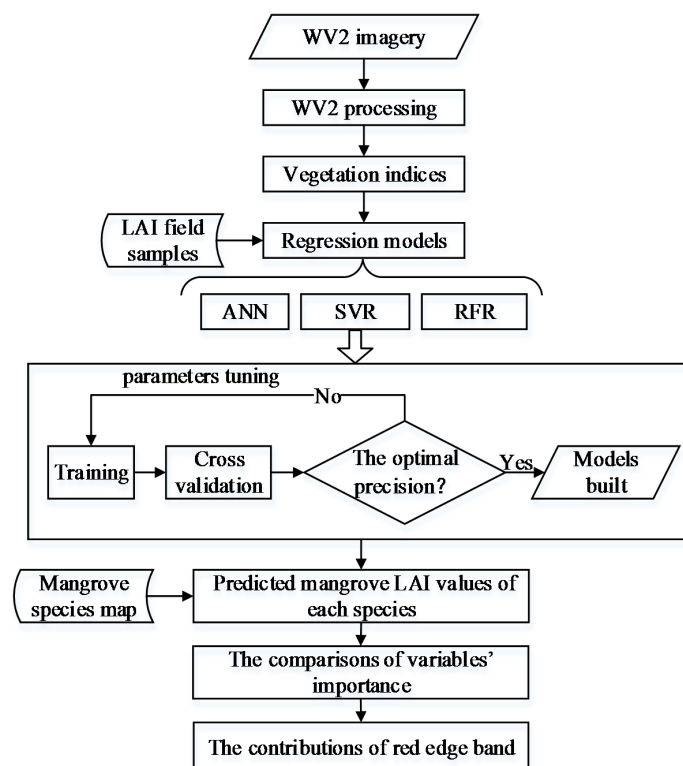


**Figure 2.** Workflow for mapping LAI using WV2 imagery and field study data.

## 2.4. Remotely Sensed Data and Processing

A WV2 multispectral image, dated on 11 November 2011, was acquired for the mangrove forests in Dawei Bay (Table 1). It contains eight multispectral bands with 2 m resolution and a panchromatic band with 0.5 m resolution. Four new bands provided by WV2 include a coastal zone band, a yellow band, a red-edge band, and a near infrared-2 band. The red-edge band has been demonstrated to be particularly more sensitive to biophysical parameters of forests than other traditional bands derived from optical images [21,50]. Consequently, WV2 imagery has high potential for application to LAI estimation of mangrove forests.

**Table 1.** The spectral band information of WV2 imagery.

Types of Bands	Wavebands	Spectral Band Edges	Spatial Resolution
The traditional bands	B2	blue band	2 m
	B3	green band	
	B5	red band	
	B7	near-infrared-1 band	
The new bands	B1	coastal band	
	B4	yellow band	
	B6	red-edge band	
	B8	near-infrared-2 band	
The panchromatic band	–	–	0.5 m

Preprocessing was conducted for the WV2 imagery, including geometric correction, radiometric calibration, and atmospheric correction. Geometric correction was executed by collecting fifteen ground control points using a UTM Zone 49 map projection. Following radiometric calibration, we used the sensor calibrating model of calibration utilities. Atmospheric correction was used to calculate apparent reflectance of the image using fast line-of-sight atmospheric analysis of the spectral hypercubes (FLAASH) model with the ENVI module [50]. The major input parameters of FLAASH were MODTRAN spectral resolution of  $15\text{ cm}^{-1}$ , mid-latitude summer model (MLS), atmospheric water vapor of  $2.9\text{ g/cm}^2$ , urban aerosol model, and DISORT streams 8 for multiscatter model of Scaled DISORT.

## 2.5. Mangrove Classification Based on WorldView-2 Imagery

Combined with prior knowledge, field interview and the characteristics of artificial planting, mangrove species types were also investigated for species classification. The training and testing samples were obtained, and the features of spatial location for each species were determined. Some species types were confused based on their spectral and texture features, such as between *K. candel* and *A. corniculatum*, between *P. australis* and *S. alterniflora* [49]. Therefore, to improve classification accuracy of mangrove species, the study area was further divided into 5 subareas based on spatial features of the different mangrove species. As shown in Figure 3, *K. candel* mainly grows in Subarea 1, *A. corniculatum* in Subarea 2 and 3, *P. australis* in subarea 3 and 4, and *S. alterniflora* in subarea 5.

The mangrove species was classified by using object-oriented classification and a SVM (Support Vector Machine) classifier. Since mangrove species is mostly homogeneous in the study area, the hard classification with SVM was used to separate species types. Object-oriented method was executed in the eCognition 9.0 software by Trimble Inc. (Sunnyvale, CA, USA), originally developed at Defniens AG. The segmentation parameters (color index, smoothness index, shape index, compactness index and scale parameter) were adjusted through repeated experiments and comparison of the segmentation results. The parameter values that produced the best visual effect with singular entities outlining objects of homogeneous appearance were selected [58]. The image object attributes, including 8 bands, vegetation index (NDVI and NDWI) and texture information (Homogeneity and Entropy from gray-level co-occurrence matrix), were calculated to train and construct the classifier.

Five subareas were classified separately by means of a SVM classifiers. The mangrove species of each subarea was classified separately using above attributes and SVM classifier based on the same optimal segmentation parameters. Half of the collected samples were used for training and the other half for validation. The accuracy was assessed by confusion matrix.

## 2.6. Calculation of VIs from WorldView-2 Imagery

Multi-spectral images have been widely used to quantify and map vegetation LAI over mangrove forests. However, the high spectral variation and shadows caused by canopy and topography may lead to challenges in developing accurate LAI estimation models [59]. It has been demonstrated that VIs have the potential of alleviating this problem [59]. The 20 VIs were calculated from the preprocessed WV2 imagery. These VIs have been demonstrated to successfully estimate and map forest structure parameters that could be crucial for LAI estimation (Table 2). The VIs were divided into three parts based on different bands according to the comparison between red-edge band and other main bands. They were used to develop models for inverting the LAI values of mangrove forests. The mean VIs, corresponding with the LAI of the plots, were calculated by the pixels of the imagery including the four vertex coordinates of each quadrant.

**Table 2.** The VIs derived from WV2 imagery.

Bands	VI	Commonly Related to	Ref.
Red-edge band (B6)	RedEdge Normalized Difference Vegetation Index $RE - NDVI_{65} = (\rho_{B6} - \rho_{B5}) / (\rho_{B6} + \rho_{B5})$	canopy foliage content, gap fraction, and senescence	
	RedEdge Simple Ratio Index $RE - SR_{65} = \rho_{B6} / \rho_{B5}$	Chlorophyll concentration and moisture content	[60]
	Modified RedEdge Simple Ratio Index $mRE - SR_{651} = (\rho_{B6} - \rho_{B1}) / (\rho_{B6} + \rho_{B1})$	precision agriculture, forest monitoring, and vegetation stress detection	
	RedEdge Normalized Difference Vegetation Index $RE - NDVI_{61} = (\rho_{B6} - \rho_{B1}) / (\rho_{B6} + \rho_{B1})$	Vegetation status, canopy structure	
	RedEdge Simple Ratio Index $RE - SR_{61} = \rho_{B6} / \rho_{B1}$	Vegetation status, canopy structure	
	Modified Chlorophyll Absorption in Reflectance Index $MCARI_{653} = [(\rho_{B6} - \rho_{B5}) - 0.2(\rho_{B6} - \rho_{B3})] \times (\rho_{B6} / \rho_{B5})$	relative abundance of chlorophyll, leaf pigments and vegetation status	[61]
	Transformed Chlorophyll Absorption in Reflectance Index $TCARI_{653} = 3[(\rho_{B6} - \rho_{B5}) - 0.2(\rho_{B6} - \rho_{B3}) \times (\rho_{B6} / \rho_{B5})]$	relative abundance of chlorophyll, leaf pigments and vegetation status	
	Triangular Vegetation Index $TVI_{653} = 0.5[120(\rho_{B6} - \rho_{B3}) - 200(\rho_{B5} - \rho_{B3})]$	Leaf pigments, vegetation status and green LAI,	
	Normalized Difference Vegetation Index $NDVI_{75} = (\rho_{B7} - \rho_{B5}) / (\rho_{B7} + \rho_{B5})$	Vegetation status, canopy structure	
	Simple Ratio Index $SRI_{75} = \rho_{B7} / \rho_{B5}$	Vegetation status, canopy structure	[62]
eeNear-infrared-1 band (B7)	Green Normalized Difference Vegetation Index $GNDVI_{73} = (\rho_{B7} - \rho_{B3}) / (\rho_{B7} + \rho_{B3})$	Leaf pigments, vegetation greenish	
	Modified Simple Ratio $MSR_{75} = [(\rho_{B7} / \rho_{B5}) - 1] / [(\rho_{B7} / \rho_{B5})^{0.5} + 1]$	Vegetation status, canopy structure	
	Modified Chlorophyll Absorption in Reflectance Index $MCARI_{753} = [(\rho_{B7} - \rho_{B5}) - 0.2(\rho_{B7} - \rho_{B3})] \times (\rho_{B7} / \rho_{B5})$	Leaf pigments, vegetation status	
	Transformed Chlorophyll Absorption in Reflectance Index $TCARI_{753} = 3[(\rho_{B7} - \rho_{B5}) - 0.2(\rho_{B7} - \rho_{B3}) \times (\rho_{B7} / \rho_{B5})]$	Leaf pigments, vegetation status	
	Optimized soil-Adjusted Vegetation Index $OSAVI_{75} = (1 + 0.6)(\rho_{B7} - \rho_{B5}) / (\rho_{B7} + \rho_{B5} + 0.16)$	soil variation in low vegetation cover,	[61]
Near-infrared-2 band (B8)	Environmental Vegetation Index $ EVI_{752} = 2.5(\rho_{B7} - \rho_{B5}) / (\rho_{B7} + 6\rho_{B5} - 7.5\rho_{B2} + 1)$	the vegetation signal in LAI regions	[63]
	Normalized Difference Vegetation Index $NDVI_{84} = (\rho_{B8} - \rho_{B4}) / (\rho_{B8} + \rho_{B4})$	Vegetation status, canopy structure	
	Simple Ratio Index $NDVI_{85} = (\rho_{B8} - \rho_{B5}) / (\rho_{B8} + \rho_{B5})$	Vegetation status, canopy structure	[60]
	Normalized Difference Vegetation Index $SRI_{84} = \rho_{B8} / \rho_{B4}$	Vegetation status, canopy structure	
	Simple Ratio Index $SRI_{85} = \rho_{B8} / \rho_{B5}$	Vegetation status, canopy structure	

## 2.7. LAI Inversion Modeling and Accuracy Assessment

The selected machine-learning algorithms, including ANNR, SVR and RFR, were used to develop the LAI model for the mangrove forests. LAI model building, tuning, and accuracy evaluation were performed using the R statistical environment for Windows using the packages neuralnet [64], e1071 [65], and randomForest [66]. Due to the limited samples, each model was built and optimized using a 5-fold cross validation (CV) instead of 10-fold cross validation [67]. Stratified random sampling was used to ensure that each subsample contains the whole range of LAI values. The 5-time results (e.g., the obtained RMSE of each process) were then averaged to calculate single accuracy estimation. Based on this method, the performance of the all three machine-learning algorithms was assessed. The sensitivities of input variables were determined by quantifying variables' importance using all three methods. The importance measures were standardized to a standard deviation [68].

Several critical tuning parameters used by all three machine-learning algorithms were examined using grid search, a brute-force approach used to optimize the performance of regression models. The adjustments for the main parameters were repeated until the model outputs reached the lowest mean RMSE during the 5-fold CV process. The model built with the lowest mean RMSE was considered optimized for LAI estimation in this study. Specific details of tuning parameters on all three algorithms are listed in the sections below.

To analyze the effective of VIs derived from red-edge band on LAI estimation accuracy, we conducted the experiments of different VIs combinations to build LAI models. We compared 5 different VIs combinations to estimate LAI accuracy, including all of 20 VIs, removing red-edge band's VIs and only using red-edge band's VIs, near-infrared-1 band's VIs and near-infrared-2 band's VIs, respectively.

### 2.7.1. Artificial Neural Network Regression (ANNR)

Artificial neural network (ANN) is a mathematical model based on the properties of biological neural networks. ANN models possess the advantages of no underlying assumptions about the input data, distributed parallel processing, resolution of nonlinear mapping, adaptive learning, and fewer required training data [69–71]. The BP ANN adopted in this study (Back-propagation neural network algorithm) is a multi-layered feed-forward network with back propagation. It was first proposed by Rumelhart et al. (1986) [56]. The BP ANN contains three layers, including the input, hidden, and output layers. Each layer has neurons connected by links, each of which signifies a weight. The learning algorithm is an iterative gradient descent training procedure and is carried out in two procedures: feed forward for input data and back propagation for errors [71]. First, the initial ANN weights are assigned randomly. The original input data are entered into the network, and processed by the three layers. If the calculated errors between output and actual values are unacceptable, the errors from the output layer are back propagated to the input layer. Then, the weights between the different layers are adjusted. This process is repeated until the errors are reduced to an acceptable level. We used two hidden layers in this study. The main tuning parameters for the network, including the number of hidden layer neurons (HLN) of the two layers and network iterations (NI), were continuously adjusted using CV and grid search. Other parameters used the default values in the “neuralnet” packages.

The Olden function from the R package “NeuralNetTools” uses Olden's algorithm (2004) to evaluate variables' relative importance [72]. This method is similar, but superior to Garson's algorithm [73] in representing true variable importance. The function deconstructed the connection weights of the ANN model—“Weights” method. The importance of each variable can be determined by the sum of all raw input-hidden and hidden-output connection weights between each input and output neuron. The importance values assigned to each variable are based directly on the sum of connection weights of the all hidden neurons. The relative importance of each connection weight is maintained in terms of both sign and magnitude.

### 2.7.2. Support Vector Regression (SVR)

Support vector machine (SVM) has a solid statistical learning theory based on the structural risk minimization (SRM) principle [57]. SVMs can be used for regression, classification, and other learning tasks. Essentially, SVMs map the original multi-dimensional space with linear, non-separable problems into a higher dimensional feature space with linear, separable feature space using the transformation of the kernel function, and they then construct a hyper plane with the maximum margin between different classes [74]. SVR is an application of SVMs. It is a linear regression function based on a high-dimensional feature space where the original input data are first mapped from a nonlinear function. Thus, an optimization problem has been converted into dual convex quadratic programming. Regressions based on the SVR algorithm use the radial basis function (RBF) kernel. The training of the SVR model using the RBF kernel requires two main tuning parameters: cost of constraint violation ( $C$ ) and gamma in kernel function ( $\gamma$ ). Increasing  $C$  will bring about larger penalties for estimation error and may lead to over-fitting of the model. The tuning parameter  $\gamma$  controls the shape of the hyper plane and may affect overall estimation accuracy. Other parameters used the default values in the “e1071” package [65].

The SVM algorithm does not provide directly a measure of variable importance. Luckily, the SVR model offers a  $\alpha$ -vector incorporating the support vectors in the “e1071” package. The variable importance measure was based on the inner product of the normalized predictor variables and the  $\alpha$ -vector proposed by Üstün et al. [75]. These positive or negative values were similar to regression coefficients, while the absolute values were the measure of variable importance [68].

### 2.7.3. Random Forest Regression (RFR)

The random forest regression algorithm (RFR) is a popular machine-learning algorithm that is largely insensitive to noisy data sets and has promising predictive capabilities for high-dimensional data set [44]. The random forest algorithm performs recursive partitioning of data sets [76], and makes no assumptions for the distribution of the input data sets [77]. It is an ensemble learning technique that combines a large number ( $n_{tree}$ ) of decision trees (DT) for classification and regression. In RFR algorithm, the number of regression trees is grown based on bootstrap samples of the original observations. Each node of the regression trees splits using a random subset of input variables ( $m_{try}$ ). The final prediction is determined by averaging the individual predictions of all regression trees. Validation dataset accuracy is determined by cross-validation (CV) for the remaining training dataset samples (out-of-bag (OOB) samples) with the random forest model. In a random forest framework, the generalization error is reduced by the randomness within the bootstrap samples of the original observations and the random selection of input predictors for splitting at nodes of each DT. The RFR tuning parameters ( $n_{tree}$  and  $m_{try}$ ) and accuracy assessments were obtained using grid search and the CV process. Other parameters used the default values in the “randomForest” package [66].

The “randomForest” package internally produces a measure of the importance of the predictor variables to optimize feature space measuring. The importance of each variable can be calculated in two different ways, including the Mean Decrease in Gini (MDG), and the Mean Decrease in Accuracy (MDA) [44]. The MDG calculates how much a variable reduces the Gini Impurity metric in a particular class, while the MDA takes into account the difference of OOB error resulting from the difference between original data set and a data set with randomly permuted variable. In this study, the relative importance of a certain variable is estimated by using MDA method.

#### 2.7.4. Accuracy Assessment

After building the models of LAI for mangrove forests, well-known error statistics were calculated to analyze the difference between the observed and predicted LAI, including root mean square error (RMSE) and relative RMSE ( $RMSE_r$ ). The computational formulas are as follows:

$$RMSE = \sqrt{\frac{1}{n} \sum_{i=1}^n (PRE_i - OBS_i)^2} \quad (1)$$

$$RMSE_r = \frac{RMSE}{\overline{OBS}} \quad (2)$$

where  $PRE_i$  and  $OBS_i$  ( $i = 1, 2, \dots, n$ ) represent the predicted and observed values at plot  $i$ , respectively;  $\overline{OBS}$  denotes the actual average of LAI; and  $n$  is the number of validation plots.

### 3. Results

#### 3.1. Mangrove Classification

The parameters of multi-resolution segmentation were determined as follows: color index (0.7), smoothness index, shape index (0.3), compactness index (0.4) and scale parameter (30). Five subareas were classified separately by means of a SVM classifier. The accuracy of the classification results was assessed based on a validation dataset obtained from field investigation (Table 3). The overall accuracy was 84.2% and the Kappa coefficient was 0.794. The mangrove species map was shown in Figure 3.

**Table 3.** Confusion matrix of mangrove species classification using object-oriented classification.

Classified Data	Reference Data								Total
	SA	AI	SAP	PA	AC	KC	AA	Mudflat	
SA	96	9	4	1	0	0	5	13	128
AI	0	155	31	0	16	1	2	0	205
SAP	0	3	367	3	0	0	4	11	388
PA	0	0	3	26	0	0	0	7	36
AC	0	0	0	0	31	0	0	0	31
KC	0	0	0	5	0	59	0	0	64
AA	0	12	4	12	0	0	28	1	57
Mudflat	0	0	6	1	0	2	0	70	79
Total	96	179	179	48	47	62	39	102	-

Over accuracy: 84.2%; Kappa: 0.794

SA—*Spartina alterniflora*; PA—*Phragmites australis*; AA—*Acrostichum aureum*; AI—*Acanthus ilicifolius*; AC—*Aegiceras corniculatum*; KC—*Kandelia candel*; SAP—*Sonneratia apetala*.

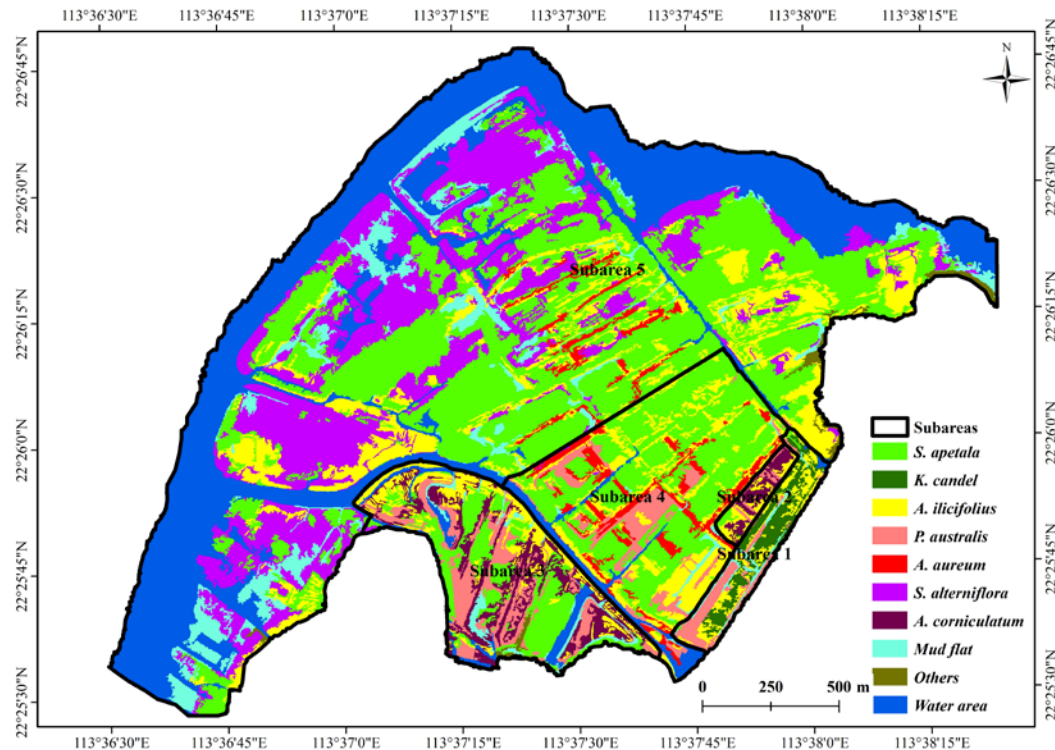


**Figure 3.** Subarea division and classification results of mangrove on Qi'ao Island.

### 3.2. Model Results and Accuracy Assessment

The optimal tuning parameters and accuracy evaluation for the different estimation models were determined by the averaged 5-fold CV RMSE and stratified random sampling, which can help reduce the bias of the validation datasets and increase stability, reliability and generalization ability of the model results [78]. As shown in Table 4, the tuning parameters were set and determined. Overall, when compared the results of different models for mangrove forest LAI estimation (Table 5), the RFR model had the best accuracy for LAI estimation. Except for the LAI model of removing VIs derived from red-edge band, the ANNR model performed slightly better than the SVR model.

We compared different VIs combinations for modeling LAI. While the inclusion of all VIs had the best accuracy, removing VIs of the red-edge band significantly decreases the accuracies of all three models (Table 5). Furthermore, the LAI model using VIs derived from red-edge band produced the better accuracy than using VIs derived from near-infrared-1 band and near-infrared-2 band.

**Table 4.** The settings and selecting values of tuning parameters using ANNR, SVR and RFR models.

Models	The Tuning Parameters	Setting Range	Interval	The Optimal Value
ANNR	HLN	2–20	2	12, 7
	NI	500–15,000	500	7000
SVR	C	$2^{-10}$ – $2^{10}$	Multiply by 2	2
	$\gamma$	$2^{-10}$ – $2^{10}$	Multiply by 2	0.03125
RFR	$n_{tree}$	100–5000	100	300
	$m_{try}$	2–20	2	12

**Table 5.** The RMSE of 5-fold CV for LAI estimation using ANNR, SVR and RFR model.

Parameters	Models	RMSEs					Average RMSE	Average RMSEr
All of VIs	ANNR	0.39	0.51	0.52	0.48	0.57	0.49	16.04%
	SVR	0.42	0.45	0.56	0.48	0.64	0.51	16.56%
	RFR	0.41	0.35	0.55	0.45	0.48	0.45	14.55%
Removing VIs Derived from red-edge band	ANNR	0.65	0.58	0.69	0.41	0.72	0.61	19.83%
	SVR	0.54	0.49	0.48	0.73	0.72	0.59	19.26%
	RFR	0.63	0.72	0.49	0.67	0.42	0.58	19.02%
VIs Derived from red-edge band	ANNR	0.53	0.58	0.67	0.75	0.50	0.60	19.57%
	SVR	0.66	0.64	0.62	0.60	0.63	0.63	20.47%
	RFR	0.64	0.65	0.73	0.44	0.42	0.58	18.71%
VIs Derived from near-infrared-1	ANNR	0.51	0.51	0.95	0.71	0.71	0.68	22.01%
	SVR	0.64	0.77	0.85	0.42	0.71	0.68	21.97%
	RFR	0.76	0.66	0.57	0.73	0.51	0.65	20.98%
VIs Derived from near-infrared-2	ANNR	0.80	0.73	0.70	0.98	0.53	0.75	24.31%
	SVR	0.79	0.89	0.84	0.54	0.86	0.78	25.38%
	RFR	0.83	0.70	0.79	0.64	0.64	0.72	23.41%

### 3.3. Variable Importance

The relative importance of input variables for LAI estimation was calculated for the ANNR, SVR and RFR models respectively. Table 6 illustrates the different VIs importance using the ANNR, SVR and RFR algorithms. The VIs derived from the red-edge band of WV2 imagery are the consistent top performers of all models. Other VIs show inconsistent performance. For SVR and RFR models, the VIs computed from Near-infrared-1 were found to be the next most important variables, followed by the near-infrared-2 band-derived VIs. However, for the ANNR model, the VIs computed from Near-infrared-2 were found to be the next most important variables, followed by the near-infrared-1 band-derived VIs.

**Table 6.** Ranking of variable importance based on the ANNR, SVR and RFR.

VIs	ANNR		SVR		RFR	
	Variable Importance	Ranks	Variable Importance	Ranks	Variable Importance	Ranks
RE-NDVI <sub>65</sub>	0.97	7	2.22	7	2.7	2
RE-SR <sub>65</sub>	2.00	2	2.44	1	3.83	1
MRE-SR <sub>651</sub>	0.03	19	2.25	5	0.69	9
RE-NDVI <sub>61</sub>	0.08	18	2.02	12	0.05	19
RE-SR <sub>61</sub>	1.32	5	2.00	15	0.17	17
MCARI <sub>653</sub>	2.14	1	2.41	2	2.59	3
TCARI <sub>653</sub>	0.09	17	1.21	20	0.04	20
TVI <sub>653</sub>	0.66	9	2.15	9	0.64	10
NDVI <sub>75</sub>	0.41	10	2.03	10	1.02	5
SRI <sub>75</sub>	0.26	12	2.26	4	0.97	6
GNDVI <sub>73</sub>	1.09	6	2.01	13	0.43	13
MSR <sub>75</sub>	0.18	15	2.28	3	1.06	4
MCARI <sub>753</sub>	0.86	8	2.21	8	0.38	15
TCARI <sub>753</sub>	0.37	11	2.24	6	0.06	18
OSAVI <sub>75</sub>	0.02	20	2.03	11	0.29	16
EVI <sub>752</sub>	0.21	14	2.00	14	0.54	12
NDVI <sub>84</sub>	0.26	13	1.51	19	0.42	14
NDVI <sub>85</sub>	1.75	3	1.71	18	0.8	8
SRI <sub>84</sub>	1.34	4	1.77	17	0.59	11
SRI <sub>85</sub>	0.13	16	1.98	16	0.89	7

### 3.4. Spatial Distribution of Mangrove Vegetation LAI

Once the models built with the highest accuracy were identified, they were used to develop LAI maps. The original WV2 images and their corresponding mangrove species maps are shown in Figure 4a,b respectively. Based on the spatial distribution patterns of the different species, we chose four typical subareas to analyze the characteristics of mangrove LAI. As shown in Figure 4c–e, the

three different models presented similar results. Further, Figure 4 shows that different mangrove species have different ranges of LAI.

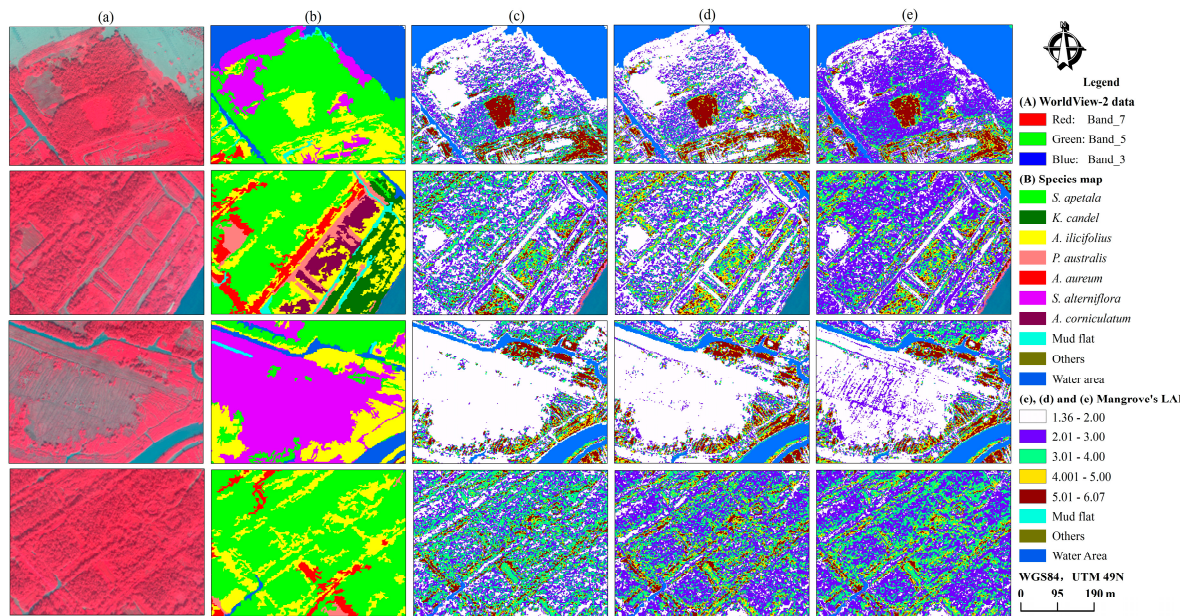


**Figure 4.** Portions of mangrove LAI maps developed using WV2 imagery and all three models: **(a)** WV2 imagery; **(b)** mangrove species classification; the LAI maps from **(c)** RFR; **(d)** ANNR and **(e)** SVR models.

The distribution of LAI values of different mangrove species are shown in Figure 5 and Table 7. The results show that different mangrove species have different ranges of LAI. *Spartina alterniflora* and *Phragmites australis* were the main herbaceous vegetation in the study area, and have the lowest LAI values with a mean of 2.02 and a range from 1.7 to 2.44, mainly because they both withered in December. They had the smallest standard deviation (SD), which indicated the lowest spatial variability. Another herbaceous species, *Acrostichum aureum*, had the highest LAI value with a mean of 2.84 and a range from 1.72 to 4.40. The evergreen *Acrostichum aureum* with a large leaf area had the highest LAI value of all studied herbaceous vegetation. The LAI of the shrub *Aegiceras corniculatum* had a mean of 2.73 with range of 1.73 to 5.55. Another shrub, *Acanthus ilicifolius*, had the highest LAI value (mean LAI of 4.51) of all the vegetation types due to its high-density canopy. Tree species (*Kandelia candel* and *Sonneratia apetala*) were the tallest in height and had the lowest canopy densities with mean values of 2.48 and 2.73. The resulting estimation map displays a high level of variation in different mangrove species.

**Table 7.** The statistics of LAI estimates for mangrove species using RFR model.

Community Types	Species	LAI Range	Mean LAI	SD
Herbaceous	<i>S. alterniflora</i>	1.70–2.44	2.02	0.30
	<i>P. australis</i>	1.73–2.42	2.02	0.27
	<i>A. aureum</i>	1.72–4.40	2.84	0.73
Shrub	<i>A. corniculatum</i>	1.73–5.55	2.73	0.86
	<i>A. ilicifolius</i>	3.10–6.06	4.51	0.92
Tree	<i>K. candel</i>	1.75–4.38	2.48	0.73
	<i>S. apetala</i>	1.74–5.35	2.73	0.86

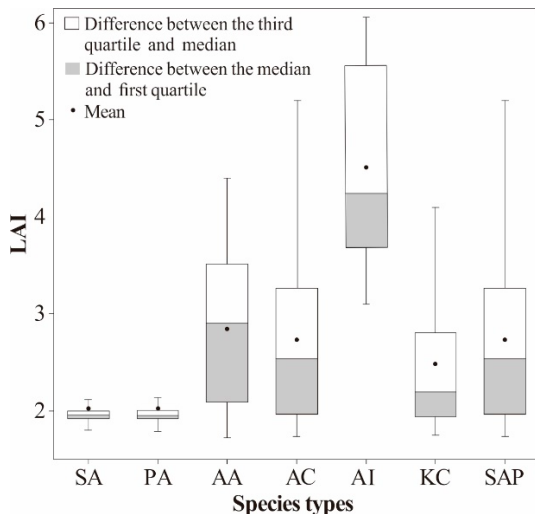


**Figure 5.** LAI distribution of mangrove species using the RFR model: SA—*Spartina alterniflora*; PA—*Phragmites australis*; AA—*Acrostichum aureum*; AI—*Acanthus ilicifolius*; AC—*Aegiceras corniculatum*; KC—*Kandelia candel*; SAP—*Sonneratia apetala*.

## 4. Discussion

### 4.1. Spatial Distribution Characteristics of LAI for Mangrove Species

The estimation models of the LAI of mangrove forests were built using all three models (RFR, ANN, and SVR) and VIs derived from WV2 imagery. The LAI estimations demonstrated a successful level of accuracy based on CV. We also predicted the spatial distribution of LAI variation and made a statistical analysis of LAI value ranges of different species types. Although there have been no previous studies in this region for comparison, the results showed that the spatial distribution of LAI values were roughly in line with the spatial distributions of different species types; consequently, the average and range of LAI for each mangrove species could be roughly produced by simply aggregating the LAI values as shown in Figure 5 and Table 7. Kovacs, Wang and Flores-Verdugo [28] mapped mangrove leaf area index at the species level using IKONOS and aggregated the LAI values to four classes (red mangrove, healthy white mangrove, poor condition white mangrove, and dead mangrove). They also demonstrated that different species types had different range of LAI values.

However, as shown in Figure 5 and Table 7, The LAI values in this region are especially suitable for the separation of the different life forms (herbaceous, shrub and tree species). The herbaceous with lowest LAI values has withered, and the shrub has more high density, consequently, with the highest LAI values, than tree species for image acquisition time dated on November [50]. However, the distinction was not complete for the same life form, such as between *S. alterniflora* and *P. australis*, and between *K. candel* and *S. apetala*.

### 4.2. Overall Performance of the LAI Model

Model testing helps select the right model, improve reliability and reduce the uncertainty in the estimating LAI of mangrove forests. Of the selected algorithms, the RFR model performed best. A major advantage of the RFR model is that it reduces the algorithm's risk for over-fitting due to relative insensitivity to variations in parameter values [44].

The ranks of variable importance are different using the selected algorithms (Table 6). That is normal due to the selected algorithms with different principles and performances. Overall, the RFR and SVR algorithms are more similar than the ANNR algorithm. That may be because the RFR and SVMR algorithms are suitable for a relatively small number of training samples than ANNR algorithm [79]. Due to the difficulties of conducting field studies in the intertidal zone, these model

properties are especially suited to research on mangrove forest inversions of biophysical parameters. Therefore, the verification results from the validation dataset demonstrated that the RFR models built for mangrove forests were well suited for LAI estimation in this study. The red-edge band-derived VIs were consistently selected as the most important band using the selected machine-learning algorithms. Consequently, we can conclude that the red-edge band is more sensitive to estimate LAI for mangrove forests than other traditional bands of multi-spectral sensors.

Mangrove forests in Dawei Bay are characterized by uneven-aged trees and exhibit high spatial variability. The spatial variability aggregated together contrasting species reflects the wide range of LAI values. The results in our studies demonstrated that the built models can be used to estimate the wide range of LAI values of aggregated together trees, shrubs and herbs species. However, we must carefully consider the restriction of the machine-learning algorithms in selection of the training and validation dataset. The main reason is that machine-learning algorithms for the parameter inversions are not able to predict or extrapolate the values beyond the range in the training dataset. Therefore, the training dataset was selected to represent the full range of potential variations using stratified random sampling [80]. Another restriction was that separate models could not be built for each mangrove species due to the limited samples in this study.

#### 4.3. Effect of the Red-Edge Band on LAI Estimation

To quantify the contribution of the red-edge band to improvement of mangrove LAI estimation, we built the 5 different LAI estimation models (Table 5). Removing eight red edge-derived VIs had consistent lower precision than all of 20 VIs based on ANNR, SVR and RFR models, respectively. Only using VIs derived from red-edge band also yield better accuracy compared with other bands, such as near-infrared-1 or near-infrared-2. Thus, the VIs calculated from the new red-edge band are more sensitive to LAI. The red-edge band can help resolve saturation of LAI estimation to some extent. When combined with the VIs of the new red-edge band and the selected algorithms, the LAI estimation models in mangrove areas had higher inversion accuracies.

Though traditional VIs of multi-spectral images, such as the normalized difference vegetation index (NDVI) or the simple ratio index (SRI), have been successfully used in LAI estimation, they have also demonstrated a lack of sensitivity to LAI variations or other biophysical parameters. Some studies have demonstrated that if the LAI exceeds 2.5, the traditional VI of the broadband spectrum is not as sensitive to the changes in LAI [55]. This is mainly because traditional broadband satellite sensors have been constrained by the asymptotic saturation of VIs due to multiple scattering of canopies from dense vegetation or high LAI [81,82]. This is particularly true for mangrove forests in our study area, where the vegetation grows very densely [50].

The results of the previous studies demonstrate the utility of red-edge band and associated VIs derived from hyperspectral [36,83] and multi-spectral images [21,39,84,85] in estimating vegetation biophysical parameters (e.g., biomass, nitrogen concentration, canopy gaps). However, some study results found that red-edge band did not have a good relation to variations in LAI using hyperspectral images [81,82]. For example, Darvishzadeh et al. suggested red-edge band was not appropriate variable for LAI estimations when aggregated together contrasting different plant species using hyperspectral images [81]. Moreover, Pu and Cheng [26] found that the red-edge band from WV2 had the worst prediction accuracy in estimating LAI of mixed natural forests compared with other WV2 MS bands due to a relatively small variation of red-edge band reflectance with a large variation of LAI. However, other studies have reported opposite findings. It was concluded that the red-edge band was the most significant determining factors for wetland vegetation LAI estimation [39]. Our findings support the latter. The results suggest that the red-edge band-derived VIs are suitable for aggregated together contrasting species in estimating LAI using WV2 imagery. It may be because the spectral features of mangrove species obtained from field investigation have more considerable variation of the albedo at ranges of 700–750 nm in our study area, compared with plant species mentioned above. A slight change of vegetation properties will lead to a notable shift in the red-edge spectral curve [39].

With the assistance of the red-edge band, the saturation problem of VIs can be alleviated to some extent in mangrove forests, thus improving the accuracy of the LAI estimation.

## 5. Conclusions

The main goals of this study were to develop accurately estimation models of LAI and explore the sensitivity of VIs of WV2 imagery in mangrove forests. Our findings show that the RFR model had the best estimation accuracy, followed by SVR. The combination of WV2 imagery and the selected machine learning algorithms were suitable for estimating the wide range of LAI values for mangrove forests. The results of spatial distribution of LAI values were roughly in line with the spatial distributions of different species types.

The study demonstrated that the spectral transformations of the red-edge band of WV2 imagery were more effective in predicting the LAI of mangrove forests than traditional bands. The red-edge band-derived VIs were consistently selected as the most important variables using different algorithms. The VIs derived from the red-edge band can improve LAI estimation accuracy by 3.79%, 2.70% and 4.47% by comparing with and without VIs derived from red-edge bands based on ANNR, SVR and RFR models, respectively.

In sum, we conclude that the combination of red-edge band and machine-learning algorithms is an effective approach for generating accurate estimates of LAIs for mangrove forests.

**Acknowledgments:** This work is supported by the National Science Foundation of China (Grant No. 41501368 and 41001291), the Science and Technology Plan Project of Guangzhou (Grant No. 201510010081), Science and Technology Research Project in Higher Education of Guangxi, China (Grant No. KY2015YB185) and the financial support of Guangxi Key Laboratory of Earth Surface Processes and Intelligent Simulation (Grant No. 2014BGERLXT13). We are also thankful to Hannes Feilhauer to provide the source code of SVMR models in this study.

**Author Contributions:** Y.Z., K.L. and L.L. designed the study, performed the experiments, analyzed the results, and wrote the manuscript. Y.Z., K.L. and S.W. conducted the field investigation and data processing. S.M., H.L. and H.Z. provided some useful suggestions to the paper's results and discussions.

**Conflicts of Interest:** The authors declare no conflict of interest.

## References

1. Alongi, D.M. Carbon sequestration in mangrove forests. *Carbon Manag.* **2012**, *3*, 313–322. [[CrossRef](#)]
2. Diele, K.; Koch, V.; Saint-Paul, U. Population structure, catch composition and cpue of the artisanally harvested mangrove crab *ucides cordatus* (ocypodidae) in the caeté estuary, north brazil: Indications for overfishing? *Aquat. Living Resour.* **2005**, *18*, 169–178. [[CrossRef](#)]
3. Das, S.; Vincent, J.R. Mangroves protected villages and reduced death toll during indian super cyclone. *Proc. Natl. Acad. Sci. USA* **2009**, *106*, 7357–7360. [[CrossRef](#)] [[PubMed](#)]
4. Zhang, K.Q. Identification of gaps in mangrove forests with airborne lidar. *Remote Sens. Environ.* **2008**, *112*, 2309–2325. [[CrossRef](#)]
5. Nagelkerken, I.; Blaber, S.J.M.; Bouillon, S.; Green, P.; Haywood, M.; Kirton, L.G.; Meynecke, J.O.; Pawlik, J.; Penrose, H.M.; Sasekumar, A.; et al. The habitat function of mangroves for terrestrial and marine fauna: A review. *Aquat. Bot.* **2008**, *89*, 155–185. [[CrossRef](#)]
6. Liu, X.P.; Li, X.; Chen, Y.M.; Tan, Z.Z.; Li, S.Y.; Ai, B. A new landscape index for quantifying urban expansion using multi-temporal remotely sensed data. *Landscape Ecol.* **2010**, *25*, 671–682. [[CrossRef](#)]
7. Ross, M.S.; Sah, J.P.; Meeder, J.F.; Ruiz, P.L.; Telesnicki, G. Compositional effects of sea-level rise in a patchy landscape: The dynamics of tree islands in the southeastern coastal everglades. *Wetlands* **2014**, *34*, S91–S100. [[CrossRef](#)]
8. Giri, C.; Ochieng, E.; Tieszen, L.L.; Zhu, Z.; Singh, A.; Loveland, T.; Masek, J.; Duke, N. Status and distribution of mangrove forests of the world using earth observation satellite data. *Glob. Ecol. Biogeogr.* **2011**, *20*, 154–159. [[CrossRef](#)]
9. Liu, K.; Li, X.; Shi, X.; Wang, S.G. Monitoring mangrove forest changes using remote sensing and gis data with decision-tree learning. *Wetlands* **2008**, *28*, 336–346. [[CrossRef](#)]

10. Ren, H.; Jian, S.G.; Lu, H.F.; Zhang, Q.M.; Shen, W.J.; Han, W.D.; Yin, Z.Y.; Guo, Q.F. Restoration of mangrove plantations and colonisation by native species in leizhou bay, south china. *Ecol. Res.* **2008**, *23*, 401–407. [[CrossRef](#)]
11. Liu, K.; Liu, L.; Liu, H.X.; Li, X.; Wang, S.G. Exploring the effects of biophysical parameters on the spatial pattern of rare cold damage to mangrove forests. *Remote Sens. Environ.* **2014**, *150*, 20–33. [[CrossRef](#)]
12. Flores-de-Santiago, F.; Kovacs, J.M.; Flores-Verdugo, F. The influence of seasonality in estimating mangrove leaf chlorophyll-a content from hyperspectral data. *Wetl. Ecol. Manag.* **2013**, *21*, 193–207. [[CrossRef](#)]
13. Laurent, V.C.E.; Schaepman, M.E.; Verhoef, W.; Weyermann, J.; Chavez, R.O. Bayesian object-based estimation of lai and chlorophyll from a simulated sentinel-2 top-of-atmosphere radiance image. *Remote Sens. Environ.* **2014**, *140*, 318–329. [[CrossRef](#)]
14. Liu, Y.; Liu, R.G.; Chen, J.M. Retrospective retrieval of long-term consistent global leaf area index (1981–2011) from combined avhrr and modis data. *J. Geophys. Res. Biogeosci.* **2012**, *117*, 1–14. [[CrossRef](#)]
15. Canisius, F.; Fernandes, R.; Chen, J. Comparison and evaluation of medium resolution imaging spectrometer leaf area index products across a range of land use. *Remote Sens. Environ.* **2010**, *114*, 950–960. [[CrossRef](#)]
16. Kovacs, J.M.; King, J.M.; Flores de Santiago, F.; Flores-Verdugo, F. Evaluating the condition of a mangrove forest of the mexican pacific based on an estimated leaf area index mapping approach. *Environ. Monit. Assess.* **2009**, *157*, 137–149. [[CrossRef](#)] [[PubMed](#)]
17. Carlson, T.N.; Ripley, D.A. On the relation between ndvi, fractional vegetation cover, and leaf area index. *Remote Sens. Environ.* **1997**, *62*, 241–252. [[CrossRef](#)]
18. Wang, L.; Sousa, W.P.; Gong, P.; Biging, G.S. Comparison of ikonos and quickbird images for mapping mangrove species on the caribbean coast of panama. *Remote Sens. Environ.* **2004**, *91*, 432–440. [[CrossRef](#)]
19. Ozdemir, I.; Karnieli, A. Predicting forest structural parameters using the image texture derived from worldview-2 multispectral imagery in a dryland forest, israel. *Int. J. Appl. Earth Obs. Geoinf.* **2011**, *13*, 701–710. [[CrossRef](#)]
20. Karlson, M.; Ostwald, M.; Reese, H.; Bazié, H.R.; Tankoano, B. Assessing the potential of multi-seasonal worldview-2 imagery for mapping west african agroforestry tree species. *Int. J. Appl. Earth Obs. Geoinf.* **2016**, *50*, 80–88. [[CrossRef](#)]
21. Adjourlolo, C.; Mutanga, O.; Cho, M.A. Estimation of canopy nitrogen concentration across c3 and c4 grasslands using worldview-2 multispectral data. *IEEE J. Sel. Top. Appl. Earth Obs. Remote Sens.* **2014**, *7*, 4385–4392. [[CrossRef](#)]
22. Ramoelo, A.; Cho, M.A.; Mathieu, R.; Madonsela, S.; Van De Kerchove, R.; Kaszta, Z.; Wolff, E. Monitoring grass nutrients and biomass as indicators of rangeland quality and quantity using random forest modelling and worldview-2 data. *Int. J. Appl. Earth Obs. Geoinf.* **2015**, *43*, 43–54. [[CrossRef](#)]
23. Deng, S.Q.; Katoh, M.; Guan, Q.W.; Yin, N.; Li, M.Y. Interpretation of forest resources at the individual tree level at purple mountain, Nanjing city, China, using worldview-2 imagery by combining gps, rs and gis technologies. *Remote Sens.* **2014**, *6*, 87–110. [[CrossRef](#)]
24. Adi, N.S.; Phinn, S.; Roelfsema, C.; Samper-Villarreal, J. Integrating field and remote sensing approaches for mapping seagrass leaf area index. In Proceedings of the 34th Asian Conference on Remote Sensing 2013 (ACRS 2013), Bali, Indonesia, 20–24 October 2013; Asian Association on Remote Sensing: Bali, Indonesia, 2013; pp. 3273–3280.
25. Kamal, M.; Phinn, S.; Johansen, K. Assessment of multi-resolution image data for mangrove leaf area index mapping. *Remote Sens. Environ.* **2016**, *176*, 242–254. [[CrossRef](#)]
26. Pu, R.L.; Cheng, J. Mapping forest leaf area index using reflectance and textural information derived from worldview-2 imagery in a mixed natural forest area in Florida, US. *Int. J. Appl. Earth Obs. Geoinf.* **2015**, *42*, 11–23. [[CrossRef](#)]
27. Pope, G.; Treitz, P. Leaf area index (lai) estimation in boreal mixedwood forest of ontario, canada using light detection and ranging (lidar) and worldview-2 imagery. *Remote Sens.* **2013**, *5*, 5040–5063. [[CrossRef](#)]
28. Kovacs, J.M.; Wang, J.; Flores-Verdugo, F. Mapping mangrove leaf area index at the species level using ikonos and lai-2000 sensors for the agua brava lagoon, mexican pacific. *Estuar. Coast. Shelf Sci.* **2005**, *62*, 377–384. [[CrossRef](#)]
29. Vaiphasa, C.; Ongsomwang, S.; Vaiphasa, T.; Skidmore, A.K. Tropical mangrove species discrimination using hyperspectral data: A laboratory study. *Estuar. Coast. Shelf Sci.* **2005**, *65*, 371–379. [[CrossRef](#)]

30. Kovacs, J.M.; Lu, X.X.; Flores-Verdugo, F.; Zhang, C.; de Santiago, F.F.; Jiao, X. Applications of alos palsar for monitoring biophysical parameters of a degraded black mangrove (*avicennia germinans*) forest. *ISPRS J. Photogramm. Remote Sens.* **2013**, *82*, 102–111. [[CrossRef](#)]
31. Kovacs, J.M.; de Santiago, F.F.; Bastien, J.; Lafrance, P. An assessment of mangroves in guinea, west africa, using a field and remote sensing based approach. *Wetlands* **2010**, *30*, 773–782. [[CrossRef](#)]
32. Kovacs, J.M.; Vandenberg, C.V.; Wang, J.; Flores-Verdugo, F. The use of multipolarized spaceborne sar backscatter for monitoring the health of a degraded mangrove forest. *J. Coast. Res.* **2008**, *24*, 248–254. [[CrossRef](#)]
33. Kovacs, J.M.; Vandenberg, C.V.; Flores-Verdugo, F. Assessing fine beam radarsat-1 backscatter from a white mangrove (*laguncularia racemosa* (gaertner)) canopy. *Wetl. Ecol. Manag.* **2006**, *14*, 401–408. [[CrossRef](#)]
34. Wong, F.K.K.; Fung, T. Combining hyperspectral and radar imagery for mangrove leaf area index modeling. *Photogramm. Eng. Remote Sens.* **2013**, *79*, 479–490. [[CrossRef](#)]
35. Horler, D.; Dockray, M.; Barber, J. The red edge of plant leaf reflectance. *Int. J. Remote Sens.* **1983**, *4*, 273–288. [[CrossRef](#)]
36. Mutanga, O.; Skidmore, A.K. Integrating imaging spectroscopy and neural networks to map grass quality in the kruger national park, south africa. *Remote Sens. Environ.* **2004**, *90*, 104–115. [[CrossRef](#)]
37. Van Deventer, H.; Cho, M.A.; Mutanga, O.; Ramoelo, A. Capability of models to predict leaf n and p across four seasons for six sub-tropical forest evergreen trees. *ISPRS J. Photogramm. Remote Sens.* **2015**, *101*, 209–220. [[CrossRef](#)]
38. Cho, M.A.; Ramoelo, A.; Debba, P.; Mutanga, O.; Mathieu, R.; van Deventer, H.; Ndlovu, N. Assessing the effects of subtropical forest fragmentation on leaf nitrogen distribution using remote sensing data. *Landsc. Ecol.* **2013**, *28*, 1479–1491. [[CrossRef](#)]
39. Mutanga, O.; Adam, E.; Cho, M.A. High density biomass estimation for wetland vegetation using worldview-2 imagery and random forest regression algorithm. *Int. J. Appl. Earth Obs. Geoinf.* **2012**, *18*, 399–406. [[CrossRef](#)]
40. Siegmann, B.; Jarmer, T. Comparison of different regression models and validation techniques for the assessment of wheat leaf area index from hyperspectral data. *Int. J. Remote Sens.* **2015**, *36*, 4519–4534. [[CrossRef](#)]
41. Houborg, R.; Boegh, E. Mapping leaf chlorophyll and leaf area index using inverse and forward canopy reflectance modeling and spot reflectance data. *Remote Sens. Environ.* **2008**, *112*, 186–202. [[CrossRef](#)]
42. Gonzalez-Sanpedro, M.C.; Le Toan, T.; Moreno, J.; Kergoat, L.; Rubio, E. Seasonal variations of leaf area index of agricultural fields retrieved from landsat data. *Remote Sens. Environ.* **2008**, *112*, 810–824. [[CrossRef](#)]
43. Schlerf, M.; Atzberger, C. Inversion of a forest reflectance model to estimate structural canopy variables from hyperspectral remote sensing data. *Remote Sens. Environ.* **2006**, *100*, 281–294. [[CrossRef](#)]
44. Breiman, L. Random forests. *Mach. Learn.* **2001**, *45*, 5–32. [[CrossRef](#)]
45. Prasad, R.; Pandey, A.; Singh, K.P.; Singh, V.P.; Mishra, R.K.; Singh, D. Retrieval of spinach crop parameters by microwave remote sensing with back propagation artificial neural networks: A comparison of different transfer functions. *Adv. Space Res.* **2012**, *50*, 363–370. [[CrossRef](#)]
46. Walthall, C.; Dulaney, W.; Anderson, M.; Norman, J.; Fang, H.L.; Liang, S.L. A comparison of empirical and neural network approaches for estimating corn and soybean leaf area index from landsat etm+ imagery. *Remote Sens. Environ.* **2004**, *92*, 465–474. [[CrossRef](#)]
47. Feilhauer, H.; Asner, G.P.; Martin, R.E. Multi-method ensemble selection of spectral bands related to leaf biochemistry. *Remote Sens. Environ.* **2015**, *164*, 57–65. [[CrossRef](#)]
48. Jachowski, N.R.A.; Quak, M.S.Y.; Friess, D.A.; Duangnamon, D.; Webb, E.L.; Ziegler, A.D. Mangrove biomass estimation in southwest thailand using machine learning. *Appl. Geogr.* **2013**, *45*, 311–321. [[CrossRef](#)]
49. Tang, H.; Liu, K.; Zhu, Y.; Wang, S.; Liu, L.; Song, S. Mangrove community classification based on worldview-2 image and svm method. *Acta Sci. Nat. Univ. Sunyatseni* **2015**, *54*, 102–111.
50. Zhu, Y.H.; Liu, K.; Liu, L.; Wang, S.G.; Liu, H.X. Retrieval of mangrove aboveground biomass at the individual species level with worldview-2 images. *Remote Sens.* **2015**, *7*, 12192–12214. [[CrossRef](#)]
51. Wu, Z.J.; Zhou, H.Y.; Ren, D.Z.; Gao, H.; Li, J.T. Processes controlling the seasonal and spatial variations in sulfate profiles in the pore water of the sediments surrounding Qi’ao Island, Pearl River Estuary, Southern China. *Cont. Shelf Res.* **2015**, *98*, 26–35. [[CrossRef](#)]

52. Li, X.; Yeh, A.G.O.; Wang, S.; Liu, K.; Liu, X.; Qian, J.; Chen, X. Regression and analytical models for estimating mangrove wetland biomass in south china using radarsat images. *Int. J. Remote Sens.* **2007**, *28*, 5567–5582. [[CrossRef](#)]
53. Piayda, A.; Dubbert, M.; Werner, C.; Vaz Correia, A.; Pereira, J.S.; Cuntz, M. Influence of woody tissue and leaf clumping on vertically resolved leaf area index and angular gap probability estimates. *For. Ecol. Manag.* **2015**, *340*, 103–113. [[CrossRef](#)]
54. Kovacs, J.M.; Flores-Verdugo, F.; Wang, J.F.; Aspden, L.P. Estimating leaf area index of a degraded mangrove forest using high spatial resolution satellite data. *Aquat. Bot.* **2004**, *80*, 13–22. [[CrossRef](#)]
55. Chen, J.M.; Cihlar, J. Retrieving leaf area index of boreal conifer forests using landsat tm images. *Remote Sens. Environ.* **1996**, *55*, 153–162. [[CrossRef](#)]
56. Rumelhart, D.E.; McClelland, J.L.; PDP Research Group. *Parallel Distributed Processing*; The MIT Press: Cambridge, MA, USA, 1986; Volume 1–2.
57. Cortes, C.; Vapnik, V. Support-vector networks. *Mach. Learn.* **1995**, *20*, 273–297. [[CrossRef](#)]
58. Wieland, M.; Pittore, M. Performance evaluation of machine learning algorithms for urban pattern recognition from multi-spectral satellite images. *Remote Sens.* **2014**, *6*, 2912–2939. [[CrossRef](#)]
59. Ruizluna, A.; Escobar, A.C.; Berlangarobles, C. Assessing distribution patterns, extent, and current condition of northwest mexico mangroves. *Wetlands* **2010**, *30*, 717–723. [[CrossRef](#)]
60. Pu, R.L.; Landry, S. A comparative analysis of high spatial resolution ikonos and worldview-2 imagery for mapping urban tree species. *Remote Sens. Environ.* **2012**, *124*, 516–533. [[CrossRef](#)]
61. Haboudane, D.; Miller, J.R.; Tremblay, N.; Zarco-Tejada, P.J.; Dextraze, L. Integrated narrow-band vegetation indices for prediction of crop chlorophyll content for application to precision agriculture. *Remote Sens. Environ.* **2002**, *81*, 416–426. [[CrossRef](#)]
62. Pena-Barragan, J.M.; Ngugi, M.K.; Plant, R.E.; Six, J. Object-based crop identification using multiple vegetation indices, textural features and crop phenology. *Remote Sens. Environ.* **2011**, *115*, 1301–1316. [[CrossRef](#)]
63. Eckert, S. Improved forest biomass and carbon estimations using texture measures from worldview-2 satellite data. *Remote Sens.* **2012**, *4*, 810–829. [[CrossRef](#)]
64. Anastasladis, A.D.; Magoulas, G.D.; Vrahatis, M.N. New globally convergent training scheme based on the resilient propagation algorithm. *Neurocomputing* **2005**, *64*, 253–270. [[CrossRef](#)]
65. Chang, C.C.; Lin, C.J. Libsvm: A library for support vector machines. *ACM Trans. Intell. Syst. Technol.* **2011**, *2*, 1–27. [[CrossRef](#)]
66. Liaw, A.; Wiener, M. Classification and regression by randomforest. *R News* **2002**, *2*, 18–22.
67. Fassnacht, F.E.; Hartig, F.; Latifi, H.; Berger, C.; Hernandez, J.; Corvalan, P.; Koch, B. Importance of sample size, data type and prediction method for remote sensing-based estimations of aboveground forest biomass. *Remote Sens. Environ.* **2014**, *154*, 102–114. [[CrossRef](#)]
68. Axelsson, C.; Skidmore, A.K.; Schlerf, M.; Fauzi, A.; Verhoef, W. Hyperspectral analysis of mangrove foliar chemistry using plsr and support vector regression. *Int. J. Remote Sens.* **2013**, *34*, 1724–1743. [[CrossRef](#)]
69. Wang, L.; Silván-Cárdenas, J.L.; Sousa, W.P. Neural network classification of mangrove species from multiseasonal ikonos imagery. *Photogramm. Eng. Remote Sens.* **2008**, *74*, 921–927. [[CrossRef](#)]
70. Liu, X.; Li, X.; Shi, X.; Wu, S.; Liu, T. Simulating complex urban development using kernel-based non-linear cellular automata. *Ecol. Model.* **2008**, *211*, 169–181. [[CrossRef](#)]
71. Rumelhart, D.E.; Hinton, G.E.; Williams, R.J. Learning representations by back-propagating errors. *Nature* **1986**, *323*, 533–536. [[CrossRef](#)]
72. Olden, J.D.; Joy, M.K.; Death, R.G. An accurate comparison of methods for quantifying variable importance in artificial neural networks using simulated data. *Ecol. Model.* **2004**, *178*, 389–397. [[CrossRef](#)]
73. Garson, G.D. *Interpreting Neural-Network Connection Weights*; Miller Freeman, Inc.: San Francisco, CA, USA, 1991; pp. 46–51.
74. Mountrakis, G.; Im, J.; Ogole, C. Support vector machines in remote sensing: A review. *ISPRS J. Photogramm. Remote Sens.* **2011**, *66*, 247–259. [[CrossRef](#)]
75. Üstün, B.; Melssen, W.J.; Buydens, L.M.C. Visualisation and interpretation of support vector regression models. *Anal. Chim. Acta* **2007**, *595*, 299–309. [[CrossRef](#)] [[PubMed](#)]
76. Pal, M. Random forest classifier for remote sensing classification. *Int. J. Remote Sens.* **2005**, *26*, 217–222. [[CrossRef](#)]

77. Zhang, J.; Huang, S.; Hogg, E.H.; Lieffers, V.; Qin, Y.; He, F. Estimating spatial variation in alberta forest biomass from a combination of forest inventory and remote sensing data. *Biogeosciences* **2014**, *11*, 2793–2808. [[CrossRef](#)]
78. Cutler, D.R.; Edwards, T.C., Jr.; Beard, K.H.; Cutler, A.; Hess, K.T.; Gibson, J.; Lawler, J.J. Random forests for classification in ecology. *Ecology* **2007**, *88*, 2783–2792. [[CrossRef](#)] [[PubMed](#)]
79. Cracknell, M.J.; Reading, A.M. Geological mapping using remote sensing data: A comparison of five machine learning algorithms, their response to variations in the spatial distribution of training data and the use of explicit spatial information. *Comput. Geosci.* **2014**, *63*, 22–33. [[CrossRef](#)]
80. Heenkenda, M.K.; Joyce, K.E.; Maier, S.W.; de Bruin, S. Quantifying mangrove chlorophyll from high spatial resolution imagery. *ISPRS J. Photogramm. Remote Sens.* **2015**, *108*, 234–244. [[CrossRef](#)]
81. Darvishzadeh, R.; Atzberger, C.; Skidmore, A.K.; Abkar, A.A. Leaf area index derivation from hyperspectral vegetation indices and the red edge position. *Int. J. Remote Sens.* **2009**, *30*, 6199–6218. [[CrossRef](#)]
82. Broge, N.H.; Leblanc, E. Comparing prediction power and stability of broadband and hyperspectral vegetation indices for estimation of green leaf area index and canopy chlorophyll density. *Remote Sens. Environ.* **2001**, *76*, 156–172. [[CrossRef](#)]
83. Adam, E.; Mutanga, O.; Abdel-Rahman, E.M.; Ismail, R. Estimating standing biomass in papyrus (*Cyperus papyrus* L.) swamp: Exploratory of in situ hyperspectral indices and random forest regression. *Int. J. Remote Sens.* **2014**, *35*, 693–714. [[CrossRef](#)]
84. Malahlela, O.; Cho, M.A.; Mutanga, O. Mapping canopy gaps in an indigenous subtropical coastal forest using high-resolution worldview-2 data. *Int. J. Remote Sens.* **2014**, *35*, 6397–6417. [[CrossRef](#)]
85. Dube, T.; Mutanga, O.; Elhadi, A.; Ismail, R. Intra-and-inter species biomass prediction in a plantation forest: Testing the utility of high spatial resolution spaceborne multispectral rapideye sensor and advanced machine learning algorithms. *Sensors* **2014**, *14*, 15348–15370. [[CrossRef](#)] [[PubMed](#)]



© 2017 by the authors. Licensee MDPI, Basel, Switzerland. This article is an open access article distributed under the terms and conditions of the Creative Commons Attribution (CC BY) license (<http://creativecommons.org/licenses/by/4.0/>).